ROYAL SOCIETY OF CHEMISTRY

PAPER

CrossMark
click for updates

Incident fluence dependent morphologies, photoluminescence and optical oxygen sensing properties of ZnO nanorods grown by pulsed laser deposition†

Xiao Liu,[a] Ye Sun,*[a] Miao Yu,*[b] Yongqi Yin,[a] Bin Yang,[a] Wenwu Cao[ac] and Michael N. R. Ashfold*[d]

ZnO nanorod (NR) samples have been prepared by 248 nm pulsed laser deposition using three different fluences, F, at the target surface. F is shown to influence the sample morphology and its photoluminescence (PL) properties. Use of large F ($\sim$4.0 J cm^{-2}) results in ZnO NRs with relatively low surface area to volume (S/V) ratio, the PL spectra of which are characterized by a weak near-UV component (I_{UV}) and a relatively intense visible (I_{vis}) emission feature attributable to the presence of zinc rich and oxygen deficient defects. Use of small F ($\sim$1.2 J cm^{-2}) yields ZnO NRs with larger S/V ratio, and a much increased I_{UV}/I_{vis} emission ratio. The O$_2$ sensing properties of these NR samples have been investigated by monitoring I_{UV} as a function of O$_2$ partial pressure, over a range of working temperatures (room temperature to 240 °C). All of the NR samples are shown to function as optical O$_2$ sensors, the responses of which are enhanced by operating at elevated temperatures, but the detailed sensitivity (and its temperature dependence) are shown to be strongly dependent on their (F-determined) S/V ratio and defect density.

1 Introduction

Zinc oxide (ZnO) nanorods (NRs) have been widely proposed for gas sensing applications (*e.g.* for oxygen, formaldehyde, nitrogen dioxide, ethanol, *etc.*[1–5]) on account of their excellent sensing performance, their large surface area to volume (S/V) ratios and the realisation that it is feasible to modify the NR morphology and surface properties. Thus far, ZnO NRs have mostly been explored as electrical sensors,[6–10] though a few groups have reported their application as optical sensors utilizing the photoluminescence (PL) properties of ZnO.[11–15] PL-based optical sensors can offer a number of notable attributes, including high sensitivity to the adsorption/desorption of a range of gases, simple device fabrication, applicability in the presence of electromagnetic radiation, capability of remote operation and, in particular, the fact that no electrical contact to the ZnO sample is required. Thus, even unsupported ZnO NRs grown on insulating substrates can be directly applied in gas sensing.

The PL of ZnO is sensitively dependent upon temperature. At room temperature (RT), the PL spectrum displays a narrow, near-band-gap (exciton-related) emission centred in the near-ultraviolet (UV) region and a broad visible band emission attributable to a range of defects and impurities.[16–19] Both emissions are sensitive to the surface condition of ZnO, and can provide explicit indications of variations in the surrounding gaseous environment. Operation at elevated temperatures (*i.e.* above RT) is a recognised route to achieving a larger sensing response in electrical ZnO sensors.[7–10,20–23] Similar improvements in gas sensing performance can be anticipated for optical ZnO sensors, but this has not been demonstrated hitherto. The large exciton binding energy of ZnO (60 meV at RT) ensures UV emission even at 400 °C, though the near-UV and, particularly, the visible emission intensities are reduced at elevated temperatures,[24,25] which could limit opportunities for optimising optical-based gas sensing by adjusting the working temperature. To date, most work on PL-based gas sensing using ZnO nanomaterials has focused on the intensity of the visible emission (I_{vis}) or the near-UV emission (I_{UV}) at RT,[11–15] though a

[a] Condensed Matter Science and Technology Institute, School of Science, Harbin Institute of Technology, Harbin 150080, China. E-mail: sunye@hit.edu.cn

[b] State Key Laboratory of Urban Water Resource and Environment, School of Chemical Engineering and Technology, Harbin Institute of Technology, Harbin 150001, China. E-mail: miaoyu_che@hit.edu.cn

[c] Materials Research Institute, The Pennsylvania State University, University Park, Pennsylvania 16802, USA

[d] School of Chemistry, University of Bristol, Bristol BS8 1TS, UK. E-mail: mike.ashfold@bristol.ac.uk

This journal is © The Royal Society of Chemistry 2015

J. Mater. Chem. C, 2015, **3**, 2557–2562 | **2557**

study from Barranco's group is a notable exception.[26] These authors used porous polycrystalline ZnO thin films and sensed the oxygen partial pressure in the environment by monitoring I_{UV} at 25 °C and 80 °C, seemingly finding a larger sensing response at the higher working temperature. However, we are unaware of any systematic examination of the temperature-dependent, I_{UV} PL-based gas sensing properties of high quality ZnO nanostructures.

Many groups have succeeded in producing high-quality ZnO NRs by pulsed laser deposition (PLD).[27–30] Such studies have shown that the NR morphologies and optical properties can be controlled by tuning growth parameters like substrate temperature (T_{sub}), oxygen partial pressure and growth duration.[31–33] Our previous PLD studies using a 193 nm excimer laser also showed that the laser fluence (F) incident on the target surface can be an important parameter when growing ZnO NRs, due to the bombardment effect of high-energy species in the ablation plume.[34] The F-dependence of the plume may also influence the number and nature of defects in (and thus the PL properties of) the as-grown NRs but, again, we are not aware of any previous reports addressing this topic.

In the present work, three types of ZnO NR – each with distinct morphologies and PL properties – have been formed by PLD using 248 nm laser radiation and three different incident fluences. The I_{UV} PL-based oxygen sensing properties of each family of NR have been investigated systematically over the temperature range RT ≤ T_{NR} ≤ 240 °C, and the effects of F and the underlying mechanisms are discussed accordingly.

2 Experimental

ZnO NRs were produced on Si(100) substrates by PLD. The output of a KrF excimer laser (Lambda-Physik COMPex 205, λ = 248 nm, pulse duration 25 ns, repetition rate 8 Hz, energy 16 mJ per pulse) was focused onto a rotating ZnO ceramic target (99.99%) mounted in an evacuable PLD chamber. The target–substrate separation was fixed at 37 mm. The sample deposition involved two steps: (1) a thin seed layer was deposited at T_{sub} = 450 °C in a low background pressure of oxygen (5 Pa) for 10 min; (2) NRs were then grown at T_{sub} = 700 °C in a background pressure of argon (70 Pa) for 90 min. The illuminated area on the target surface was varied by adjusting the position of the focusing lens: spot sizes of ~0.4 mm^2, ~0.9 mm^2 and ~1.3 mm^2 (which translate into incident fluences, $F \sim$ 4.0 J cm^{-2}, ~1.8 J cm^{-2} and ~1.2 J cm^{-2}) were used for growing the three ZnO NR types, which we henceforth denote as type A (TA), B (TB) and C (TC) samples. Depositions at still lower F (~1 J cm^{-2}) yielded only a low density of nanoparticles. The morphology and crystallinity of the as-grown TA, TB and TC NRs were characterized by field emission scanning electron microscopy (FESEM, FEI Quanta 200F), high-resolution transmission electron microscopy (HRTEM, FEI, Tecnai-G2-F30) and X-ray diffraction (XRD, PANalytical, X'Pert Pro, with Cu Kα radiation). The samples were mounted in a specially designed vacuum mini-chamber (volume: 1.6 L) mounted within a spectro-fluorometer (HORIBA, Fluoromax-4, 325 nm excitation) for PL and optical gas sensing measurements. The mini-chamber was equipped with a

temperature-controlled heating system and two quartz windows, and connected to a gas flow control system *i.e.* a gas mixing chamber with two mass flow controllers (maximum flow 10 standard litres per minute (SLM) N$_2$ equivalent) and a rotary pump (providing an (air) pumping speed of 4 L s^{-1}). This system allowed strict control of the sample temperature, T_{NR}, and gas composition within the chamber – separately or simultaneously. The PL properties of the respective NR samples were measured over the temperature range RT ≤ T_{NR} ≤ 240 °C, at a pressure of 1 bar. Using the spectro-fluorometer in 'kinetics' mode allowed the emission intensity at any particular wavelength to be monitored with 1 s time resolution – thereby enabling dynamic investigation of the PL-based gas sensing properties of the various ZnO samples. In the optical gas sensing measurements that follow, we focus on the maximum absolute count rates in the UV and visible regions of the PL spectrum (which we identify as $I_{UV(max)}$ and $I_{vis(max)}$).

3 Results and discussion

Use of $F \sim$ 4.0 J cm^{-2}, ~1.8 J cm^{-2} and ~1.2 J cm^{-2} results in three distinct types of ZnO NR sample, as revealed by the top and cross-sectional view SEM images shown in Fig. 1a–f. The TA sample grown with $F \sim$ 4.0 J cm^{-2} comprises a densely-packed array of NRs with average length $\ell \sim$ 500 nm and diameter $d \sim$ 170 nm (Fig. 1a and b). Use of $F \sim$ 1.8 J cm^{-2} yields a lower density array of poorly aligned NRs with $\ell \sim$ 900 nm and $d \sim$ 160 nm (TB sample, Fig. 1c and d). The vertical alignment of the NRs improves upon decreasing F further, to ~1.2 J cm^{-2}; as Fig. 1e and f shows, the TC NR sample is characterised by $\ell \sim$ 600 nm and $d \sim$ 85 nm. Histograms showing the distributions of TA, TB and TC NR diameters are included as (ESI, Fig. S1†). The XRD data shown in Fig. S2† serves to confirm the relative alignments of the NRs; only the ZnO (002) peak is evident in the spectra of the TA and TC samples, whereas the (100) and (101) peaks are also clearly evident in the XRD spectrum of the TB sample. TEM and HRTEM images of a TC NR with d = 80 nm are presented in Fig. 1g and h. The measured lattice spacing of 0.52 nm (characteristic of wurtzite ZnO(001)) confirms that the NRs grow along the c-axis direction.

All of these data point to the important influence of F in the growth and morphology of ZnO NRs grown by PLD at 248 nm, consistent with prior illustrations of F-dependent effects when using a laser wavelength of 193 nm.[34] The earlier study suggested that F determines not only the quantity but also the composition and the energy distribution of material in the plume formed in the ablation event. Plumes formed at higher F contain a larger flux of high energy species (*e.g.* Zn^{2+} and Zn$^+$ ions) which bombard the pre-formed ZnO sample, modifying its morphology and influencing growth: as a result, thicker (thinner) NRs are obtained when using higher (lower) F.[34]

The PL properties of ZnO NRs are intimately related to their crystal quality, defects, and morphology.[17,35–38] Fig. 2 presents PL spectra obtained following 325 nm illumination of equal areas of TA, TB and TC samples measured at RT in air. All three spectra show a narrow near-band-gap UV emission centred at ~380 nm and a broad visible band emission attributable to the
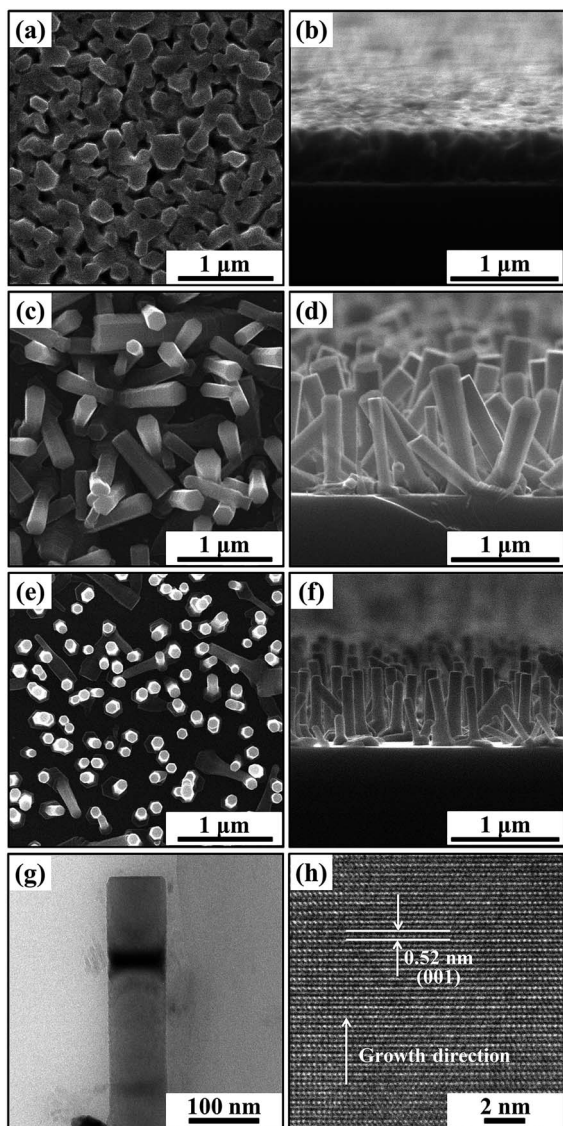
2558 | *J. Mater. Chem. C*, 2015, **3**, 2557–2562

This journal is © The Royal Society of Chemistry 2015

Fig. 1 Top view and cross-sectional view SEM images of TA (a and b), TB (c and d) and TC (e and f) NR samples. Panels (g and h) show TEM and HRTEM images of a TC nanorod.

Fig. 2 PL spectra of ZnO nanorods grown with $F \sim 4.0$ J cm^{-2} (TA sample), ~ 1.8 J cm^{-2} (TB sample) and ~ 1.2 J cm^{-2} (TC sample). The inset shows the same PL spectra normalized to the same peak I_{UV}.

presence of defects and interstitials,[16,17] but the I_{UV} to I_{vis} emission ratios are very different. The TA sample grown at highest F presents the weakest I_{UV} but the strongest I_{vis}. Green and blue emissions centred at ~ 530 nm and ~ 450 nm can be identified in the latter; these are normally attributed to defects associated with oxygen vacancies and zinc interstitials, respectively.[16,17,39,40] The TB sample (grown at lower F) shows much enhanced I_{UV} and reduced I_{vis}, while the TC sample (grown at the lowest F) shows a further large increase in I_{UV}, a modest increase in I_{vis} and much the largest I_{UV}/I_{vis} ratio. These trends all imply that lower F favours growth of ZnO NRs with higher crystal quality, which is logical in light of the foregoing discussion. In the case of the TA sample, the large F-induced bombardment effect and the significant difference in the mass of Zn and O atoms results in many oxygen-deficient-related defects – consistent with the comparatively weak I_{UV} and strong
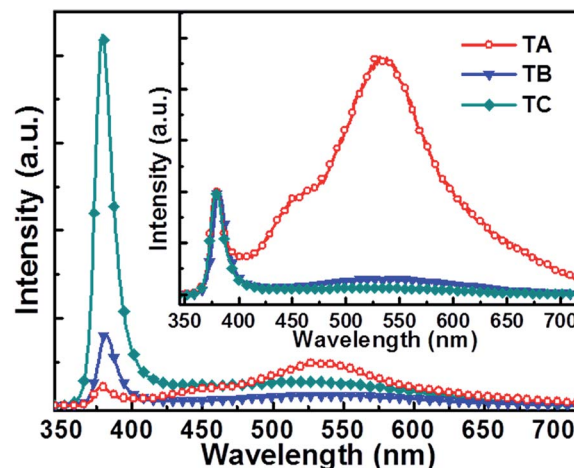
I_{vis} emissions. As many as four different factors may contribute to the differences in the PL spectra of the TB and TC samples: (a) the lower F used to grow the TC sample should favour better crystal quality; (b) the smaller average diameter of the TC sample ($d \sim 85$ nm *vs.* ~ 160 nm) may introduce a relatively greater proportion of surface defects; (c) the penetration depth (*i.e.* the distance over which the incident 325 nm light intensity drops by a factor of $1/e$) in ZnO is ~ 60 nm;[41] and (d) the NR diameter dependent re-absorption of the UV emission at 380 nm.[42] Factors (a), (c) and (d) account for the much enhanced I_{UV} and the improved I_{UV}/I_{vis} ratio exhibited by the TC sample, while factor (b) may well account for the slight increase in I_{vis} from the TC sample (*cf.* the TB sample). We also note that the 'blue' emission apparent from the TA sample is absent in the PL spectra of the TB and TC samples, reinforcing the view that F has a major influence on the number and nature of defects (and the PL properties) of ZnO samples grown by PLD.

To explore the temperature dependent gas sensing properties of ZnO NRs we first studied the PL of the TA, TB and TC NRs in pure nitrogen (N$_2$) across the range RT $\leq T_{NR} \leq 240$ °C. As Fig. 3 shows, the near-UV emission from all three samples broadens, declines in intensity and shows an obvious red shift with increasing T_{NR} – consistent with previous findings.[24,25,43] These trends in I_{UV} from ZnO NRs within this range have been successfully explained in terms of free exciton emission and an increased role for electron–phonon coupling with increasing temperature.[44,45] As Fig. 3a shows, raising T_{NR} to 150 °C reduces $I_{vis(max)}$ from the TA sample to just 4.7% of its RT value, whereas $I_{UV(max)}$ only shows a ~ 2-fold reduction. TB and TC samples show qualitatively similar T_{NR}-dependent trends in emission behaviour, and similar behaviour has been reported previously.[25] Thus we conclude that the near-UV emission is a better choice (*cf.* the visible emission) for studies of the optical gas sensing properties of ZnO NRs at elevated temperatures.

The oxygen sensing properties of all three types of NR sample were examined by monitoring I_{UV} at temperatures across the range RT $< T_{NR} < 240$ °C. Fig. 3, S3 and S4† confirm that the PL
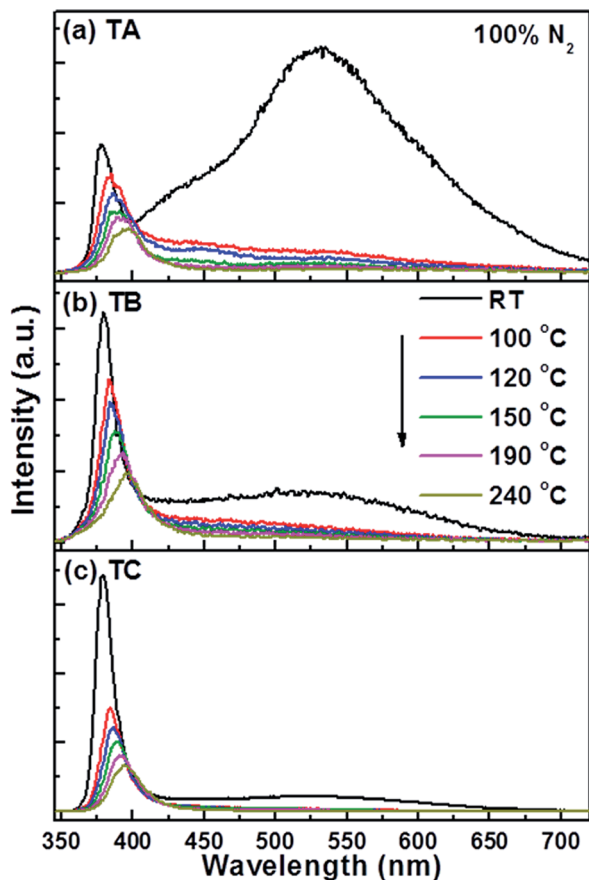
This journal is © The Royal Society of Chemistry 2015

J. Mater. Chem. C, 2015, **3**, 2557–2562 | **2559**

Fig. 3 PL spectra of (a) TA, (b) TB and (c) TC NR samples in 100% N_2 at various different temperatures in the range RT $\leq T_{NR} \leq$ 240 °C.
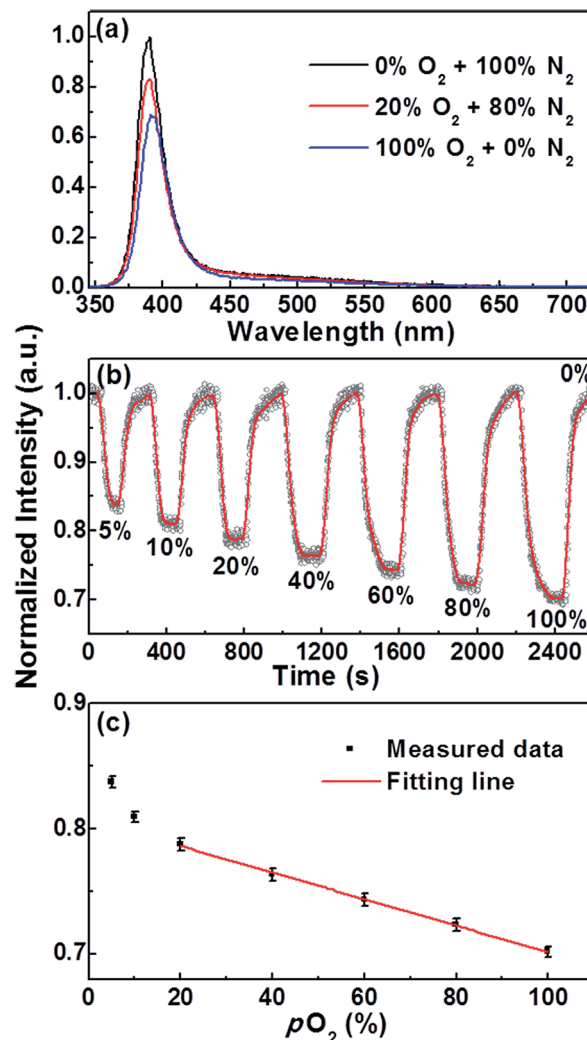

Fig. 4 (a) PL spectra of a TC NR sample measured at T_{NR} = 150 °C in the presence of 100% N_2, 20% O_2/80% N_2 and 100% O_2. (b) Dynamic $I_{UV(max)}$ response of the TC NR sample to various pO_2 at T_{NR} = 150 °C. (c) $I_{UV(max)}$ from the TC NR sample measured as a function of pO_2 at T_{NR} = 150 °C.

profile measured from a given NR sample at any particular T_{NR} is rather insensitive to replacing N_2 with O_2. The PL intensities are much more sensitive to this substitution, however. Fig. 4a presents PL spectra from the TC NR sample measured at T_{NR} = 150 °C and 1 bar pressure in 100% N_2, in a 20% O_2/80% N_2 mixture and in 100% O_2. I_{UV} clearly declines with increasing O_2 partial pressure (pO_2), in a repeatable manner (see Fig. S5†). Fig. 4b illustrates the dynamic $I_{UV(max)}$ response of a TC NR sample to various pO_2, revealing a linear $I_{UV(max)}$–pO_2 relationship across the range $20 \leq pO_2 \leq 100\%$, as shown in Fig. 4c. The measured response and recovery times are of the order of 1 min. and, within the T_{NR} range of current interest, decrease with increasing T_{NR} (see Fig. S6†). These results clearly demonstrate that the I_{UV} component within the PL of such ZnO NRs can be used for oxygen gas sensing at elevated temperatures.

T_{NR}-dependent responses, R, (defined as $R = (I_0 - I_{100})/I_0$, where I_0 and I_{100} are the $I_{UV(max)}$ values measured at pO_2 = 0% and 100%, respectively) of TA, TB and TC NR samples are shown in Fig. 5. For all three sample types, R increases linearly up to $T_{NR} \sim$ 150 °C, then starts to plateau (in the case of the TA sample) or to turnover (TB and TC samples). Within the linear range, the TC NR sample consistently gives the largest response, increasing from $R \sim 7.4\%$ at RT to $R \sim 30.7\%$ at T_{NR} = 150 °C.

To account for the different T_{NR}-dependent responses shown in Fig. 5 we need to understand the mechanisms for gas sensing

via the I_{UV} component within the PL spectrum of ZnO. Whereas the I_{vis} component is associated with both bulk- and surface-related defects, the near-UV emission (at the temperatures of current interest) is considered to derive from free excitons[44,45] in the inner part of the NR, beneath the electron-depletion layer.[46,47] The adsorption/desorption of different gas species on the ZnO surface can trap or release electrons, thereby expanding or reducing the depletion layer and influencing I_{UV}. Three factors that are likely to influence the T_{NR}-response of the various NR types are proposed:

(i) The S/V ratio. Given the measured average diameters and lengths of the three types of NR, and the high packing density of the TA NRs, we conclude that the TC NR samples present the largest (and the TA NR samples the lowest) S/V ratio;

(ii) The native surface defects. Material deposited at higher F (i.e. the TA NR sample) contains a higher defect density (e.g. oxygen vacancies, recall Fig. 2a), which may be beneficial for the dissociative adsorption of oxygen;[5]
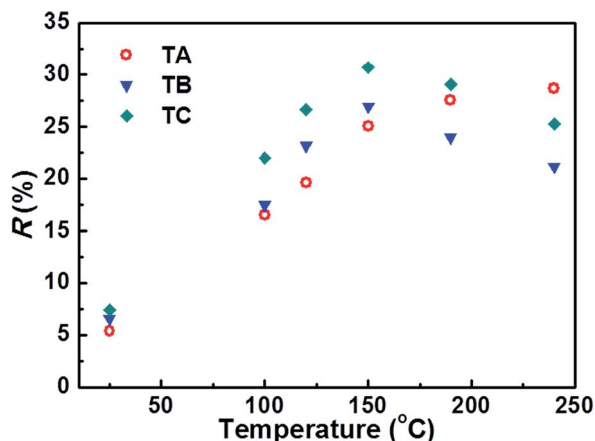
2560 | J. Mater. Chem. C, 2015, 3, 2557–2562

This journal is © The Royal Society of Chemistry 2015

Fig. 5 Working temperature (T_{NR}) dependent $I_{UV(max)}$ responses of the TA, TB and TC NR samples in a 100% O_2 atmosphere.

(iii) The competition between environmental O_2 and pre-adsorbed species. The O_2 adsorption probability can be sensitive to pre-adsorbed species, *e.g.* water molecules,[48] the desorption of which could provide free sites for O_2 adsorption. Previous studies report loss of physisorbed and chemisorbed water molecules from ZnO surfaces at temperatures ~100 °C and ~220–270 °C, respectively.[49] T_{NR} can thus be expected to play an important role in the competition between O_2 and pre-adsorbed species.

Overall, therefore, it is tempting to attribute the maximum in the O_2 sensing response shown by TC NRs at $T_{NR} \sim 150$ °C to a combination of high S/V ratio and the desorption of physisorbed water molecules. As Fig. 5 shows, the TA NRs show a subtly different O_2 sensing response, peaking at higher T_{NR} ($\geq$250 °C). These NRs have a much higher (oxygen-deficient) defect density and it is plausible that this response reflects a combination of desorption of pre-adsorbed surface species (*e.g.* water molecules), as before, and progressive O_2-induced compensation of these defects with increasing T_{NR}.

4　Conclusions

Three distinct types of ZnO NR sample have been produced by 248 nm PLD at different incident fluences, F. The TC NR samples grown at lowest F ($\sim$1.2 J cm^{-2}) are well aligned and have high S/V ratio. These thin NRs ($d \sim 85$ nm) are of high crystal quality (as evidenced by HRTEM) and give a PL spectrum with high I_{UV}/I_{vis} ratio. Conversely, TA NR samples grown at the highest F ($\sim$4.0 J cm^{-2}) have relatively small S/V ratio. The associated PL spectra show a relative weak I_{UV} band but strong I_{vis} – indicating a much higher (oxygen-deficient) defect density. The O_2 sensing properties of the three types of NR sample have been explored by monitoring I_{UV} at several different temperatures in the range RT $\leq T_{NR} \leq 240$ °C. All three samples offer an O_2 sensing capability, the sensitivity of which is increased by working at elevated temperature. The TC sample is found to exhibit the maximum O_2 sensing response, at $T_{NR} \sim 150$ °C – a result attributed to (i) the high S/V ratio, and the progressive

desorption of competing pre-adsorbed species (*e.g.* physisorbed water molecules) with increasing T_{NR}. The present study provides deeper insights into both the growth (by PLD) and gas sensing properties of ZnO NRs, and could be extended to encompass PLD growth of other types of material, and to further investigation of the ability of ZnO NRs to sense other gases.

Notes and references

1　S. M. Niu, Y. F. Hu, X. N. Wen, Y. S. Zhou, F. Zhang, L. Lin, S. H. Wang and Z. L. Wang, *Adv. Mater.*, 2013, **25**, 3701–3706.
2　S. M. Wang, Z. F. Li, P. Wang, C. H. Xiao, R. Zhao, B. X. Xiao, T. Y. Yang and M. Z. Zhang, *CrystEngComm*, 2013, **16**, 5716–5723.
3　C. W. Na, H. S. Woo, I. D. Kim and J. H. Lee, *Chem. Commun.*, 2011, **47**, 5148–5150.
4　C. P. Gu, S. S. Li, J. R. Huang, C. C. Shi and J. H. Liu, *Sens. Actuators, B*, 2013, **177**, 453–459.
5　M. J. S. Spencer, *Prog. Mater. Sci.*, 2012, **57**, 437–486.
6　O. Lupan, V. V. Ursaki, G. Chai, L. Chow, G. A. Emelchenko, I. M. Tiginyanu, A. N. Gruzintsev and A. N. Redkin, *Sens. Actuators, B*, 2010, **144**, 56–66.
7　N. Qin, Q. Xiang, H. B. Zhao, J. C. Zhang and J. Q. Xu, *CrystEngComm*, 2014, **16**, 7062–7073.
8　S. Q. Tian, F. Yang, D. W. Zeng and C. S. Xie, *J. Phys. Chem. C*, 2012, **116**, 10586–10591.
9　H. N. Hieu, N. M. Vuong, H. Jung, D. M. Jang, D. Kim, H. Kim and S.-K. Hong, *J. Mater. Chem.*, 2012, **22**, 1127–1134.
10　D. Zappa, E. Comini and G. Sberveglieri, *Nanotechnology*, 2013, **24**, 444008.
11　C. Baratto, S. Todros, G. Faglia, E. Comini, G. Sberveglieri, S. Lettieri, L. Santamaria and P. Maddalena, *Sens. Actuators, B*, 2009, **140**, 461–466.
12　D. Valerini, A. Cretì, A. P. Caricato, M. Lomascolo, R. Rella and M. Martino, *Sens. Actuators, B*, 2010, **145**, 167–173.
13　A. Cretì, D. Valerini, A. Taurino, F. Quaranta, M. Lomascolo and R. Rella, *J. Appl. Phys.*, 2012, **111**, 073520.
14　R. Aad, V. Simic, L. L. Cunff, L. Rocha, V. Sallet, C. Sartel, A. Lusson, C. Couteau and G. Lerondel, *Nanoscale*, 2013, **5**, 9176–9180.
15　D. Padilla-Rueda, J. M. Vadillo and J. J. Laserna, *Appl. Surf. Sci.*, 2012, **259**, 806–810.
16　B. X. Lin, Z. X. Fu and Y. B. Jia, *Appl. Phys. Lett.*, 2001, **79**, 943–945.
17　A. B. Djurišić and Y. H. Leung, *Small*, 2006, **2**, 944–961.

18 T. M. Børseth, B. G. Svensson, A. Y. Kuznetsov, P. Klason, Q. X. Zhao and M. Willander, *Appl. Phys. Lett.*, 2006, **89**, 262112.

19 Y. Yin, Y. Sun, M. Yu, X. Liu, B. Yang, D. Liu, S. Liu, W. Cao and M. N. R. Ashfold, *RSC Adv.*, 2014, **4**, 44452–44456.

20 M. Amin, N. M. Shah, A. S. Bhatti and M. A. Malik, *CrystEngComm*, 2014, **16**, 6080–6088.

21 H. S. Woo, C. H. Kwak, I. D. Kim and J. H. Lee, *J. Mater. Chem. A*, 2014, **2**, 6412–6418.

22 M. R. Alenezi, S. J. Henley, N. G. Emerson and S. R. P. Silva, *Nanoscale*, 2014, **6**, 235–247.

23 W. Wen, J. M. Wu and Y. D. Wang, *Appl. Phys. Lett.*, 2012, **100**, 262111.

24 M. Omari, A. Gupta and N. Kouklin, *J. Appl. Phys.*, 2010, **108**, 024315.

25 A. Gupta, M. Omari and N. Kouklin, *Phys. Status Solidi C*, 2009, **6**, 607–609.

26 J. R. Sanchez-Valencia, M. Alcaire, P. Romero-Gómez, M. Macias-Montero, F. J. Aparicio, A. Borras, A. R. Gonzalez-Elipe and A. Barranco, *J. Phys. Chem. C*, 2014, **118**, 9852–9859.

27 G. M. Fuge, T. M. S. Holmes and M. N. R. Ashfold, *Chem. Phys. Lett.*, 2009, **479**, 125–127.

28 P. Zhang, G. D. Zhou, H. B. Gong, H. Y. Xu, D. Nakamura, T. Okada, H. B. Zeng and B. Q. Cao, *Sci. Adv. Mater.*, 2012, **4**, 455–462.

29 R. P. Doherty, Y. Sun, Y. Sun, J. L. Warren, N. A. Fox, D. Cherns and M. N. R. Ashfold, *Appl. Phys. A: Mater. Sci. Process.*, 2007, **89**, 49–55.

30 C. V. Varanasi, K. D. Leedy, D. H. Tomich, G. Subramanyam and D. C. Look, *Nanotechnology*, 2009, **20**, 385706.

31 L. C. Tien, S. J. Pearton, D. P. Norton and F. Ren, *J. Mater. Sci.*, 2008, **43**, 6925–6932.

32 Z. W. Liu, C. K. Ong, T. Yu and Z. X. Shen, *Appl. Phys. Lett.*, 2006, **88**, 053110.

33 Y. Sun, G. M. Fuge and M. N. R. Ashfold, *Chem. Phys. Lett.*, 2004, **396**, 21–26.

34 Y. Sun, R. P. Doherty, J. L. Warren and M. N. R. Ashfold, *Chem. Phys. Lett.*, 2007, **447**, 257–262.

35 D. Zhao, X. X. Zhang, H. B. Dong, L. J. Yang, Q. S. Zeng, J. Z. Li, L. Cai, X. Zhang, P. S. Luan and Q. Zhang, *Nanoscale*, 2013, **5**, 4443–4448.

36 H. P. He, Q. A. Yang, C. Liu, L. W. Sun and Z. Z. Ye, *J. Phys. Chem. C*, 2011, **115**, 58–64.

37 Y. Sun, G. M. Fuge, N. A. Fox, D. J. Riley and M. N. R. Ashfold, *Adv. Mater.*, 2005, **17**, 2477–2481.

38 Y. Sun and M. N. R. Ashfold, *Nanotechnology*, 2007, **18**, 245701.

39 H. Zeng, G. Duan, Y. Li, S. Yang, X. Xu and W. Cai, *Adv. Funct. Mater.*, 2010, **20**, 561–572.

40 D. H. Zhang, Z. Y. Xue and Q. P. Wang, *J. Phys. D: Appl. Phys.*, 2002, **35**, 2837–2840.

41 J. F. Muth, R. M. Kolbas, A. K. Sharma, S. Oktyabrsky and J. Narayan, *J. Appl. Phys.*, 1999, **85**, 7884.

42 I. Hussain, N. Bano, S. Hussain, Y. Soomro, O. Nur and M. Willander, *Materials*, 2011, **4**, 1260–1270.

43 D. Zhao, C. Zhang, X. X. Zhang, L. Cai, X. Zhang, P. S. Luan, Q. Zhang, M. Tu, Y. C. Wang, W. Y. Zhou, Z. Y. Li and S. S. Xie, *Nanoscale*, 2014, **6**, 483–491.

44 A. Gupta, M. Omari and N. Kouklin, *J. Appl. Phys.*, 2008, **103**, 124312.

45 X.-B. Chen, J. Huso, J. L. Morrison and L. Bergman, *J. Appl. Phys.*, 2007, **102**, 116105.

46 X. Liu, X. H. Wu, H. Cao and R. P. H. Chang, *J. Appl. Phys.*, 2005, **95**, 3141.

47 Y. Sun, N. G. Ndifor-Angwafor, D. J. Riley and M. N. R. Ashfold, *Chem. Phys. Lett.*, 2006, **431**, 352–357.

48 H. Noei, H. Qiu, Y. Wang, E. Löffler, C. Wöll and M. Muhler, *Phys. Chem. Chem. Phys.*, 2008, **10**, 7092–7097.

49 K. Morishige, S. Kittaka, T. Moriyasu and T. Morimoto, *J. Chem. Soc., Faraday Trans. 1*, 1980, **76**, 738–745.

2562 | *J. Mater. Chem. C*, 2015, **3**, 2557–2562

This journal is © The Royal Society of Chemistry 2015